SAPHIRA detector for infrared wavefront sensing

Gert Finger[a], Ian Baker[b], Domingo Alvarez [a], Derek Ives[a], Leander Mehrgan[a], Manfred Meyer[a], Jörg Stegmeier[a] and Harald J. Weller[b].
[a]European Southern Observatory, Karl Schwarzschildstrasse 2, D-85748-Garching, Germany.
[b] Selex ES Ltd, Southampton, Hants, SO15 OLG, UK.

ABSTRACT

The only way to overcome the CMOS noise barrier of near infrared sensors used for wavefront sensing and fringe tracking is the amplification of the photoelectron signal inside the infrared pixel by means of the avalanche gain. In 2007 ESO started a program at Selex to develop near infrared electron avalanche photodiode arrays (eAPD) for wavefront sensing and fringe tracking. In a first step the cutoff wavelength was reduced from 4.5 micron to 2.5 micron in order to verify that the dark current scales with the bandgap and can be reduced to less than one electron/ms, the value required for wavefront sensing. The growth technology was liquid phase epitaxy (LPE) with annular diodes based on the loophole interconnect technology. The arrays required deep cooling to 40K to achieve acceptable cosmetic performance at high APD gain. The second step was to develop a multiplexer tailored to the specific application of the GRAVITY instrument wavefront sensors and the fringe tracker. The pixel format is 320x256 pixels. The array has 32 parallel video outputs which are arranged in such a way that the full multiplex advantage is available also for small subwindows. Nondestructive readout schemes with subpixel sampling are possible. This reduces the readout noise at high APD gain well below the subelectron level at frame rates of 1 KHz. The third step was the change of the growth technology from liquid phase epitaxy to metal organic vapour phase epitaxy (MOVPE). This growth technology allows the band structure and doping to be controlled on a 0.1µm scale and provides more flexibility for the design of diode structures. The bandgap can be varied for different layers of $Hg_{(1-x)}Cd_xTe$. It is possible to make heterojunctions and apply solid state engineering techniques. The change to MOVPE resulted in a dramatic improvement in the cosmetic quality with 99.97 % operable pixels at an operating temperature of 85K. Currently this sensor is deployed in the 4 wavefront sensors and in the fringe tracker of the VLT instrument GRAVITY. Initial results will be presented. An outlook will be given on the potential of APD technology to be employed in large format near infrared science detectors. Several of the results presented here have also been shown to a different audience at the Scientific Detector Workshop in October 2013 in Florence but this paper has been updated with new results [1].

Keywords: avalanche photodiode, eAPD, HgCdTe, readout noise, excess noise, APD gain, cryogenic amplifier, infrared, wavefront sensor, fringe tracker

1. INTRODUCTION

Until now the performance of infrared wavefront sensors and fringe trackers was based on CMOS detectors operating in the capacitive discharge mode with a source follower in the unit cell. Due to the high analog bandwidth required to achieve frame rates of 1 kHz the readout noise severely limits the sensitivity. Typical noise figures at pixel rates of 5 MHz per video output are ~70 electrons rms. In the past decade improvements in CMOS technology has only marginally reduced this noise figure. This impasse can be broken if the signal is amplified before it is integrated onto the silicon readout. Silicon amplifiers are not practical in small pixel sizes so attention has turned to electron multiplication by an impact ionisation effect – the so-called avalanche photodiode array (APD). The need for low breakdown currents at high voltages requires a mature device technology. Hence, developments in a number of companies over the past 5 years have now made these devices available to the astronomy community.

Since HgCdTe, contrary to silicon, is a direct semiconductor, phonons are not needed to generate an electron-hole pair. Furthermore, in HgCdTe the mass of the electron is much smaller than the mass of the holes and the gain process is then mainly due to pure electron multiplication. Therefore, the APD gain process in HgCdTe is almost noiseless [2][3]. Noise figures of 1.2 have been measured at an APD gain of 80 whereas the intrinsic noise figure in silicon is greater than 2.

Adaptive Optics Systems IV, edited by Enrico Marchetti, Laird M. Close, Jean-Pierre Véran, Proc. of SPIE Vol. 9148, 914817 · © 2014 SPIE
CCC code: 0277-786X/14/$18 · doi: 10.1117/12.2057078

The ultimate limit for the noise equivalent photon flux at high APD gain and negligible readout noise is the ratio of the noise figure and the quantum efficiency. High quantum efficiency in HgCdTe has been demonstrated in many applications. Hence, HgCdTe has the potential to outperform silicon even at optical wavelengths

Avalanche gain has already been used successfully to enhance the sensitivity in laser gated imaging applications. To achieve high APD gain the cut-off wavelength of the HgCdTe material used for these applications is 4.5 μm. This is possible because the integration times for laser gated imaging are in the hundred nanosecond range, whereas wavefront sensing requires integration times of 1 ms. In order to reduce the dark current, first prototype arrays have been made with a lower cutoff wavelength of λ_c ~2.5 μm. Tests on an already existing multiplexer demonstrated that the dark current is made sufficiently small for integration times of 1ms [9]. It then became evident that a special ROIC had to be designed to meet the needs of fringe tracking and wavefront sensing. This ROIC is called SAPHIRA. Initial LPE grown devices did not reproduce the performance of the prototypes. Widening the depletion region delivered good LPE SAPHIRA devices, which operate best at temperatures of T=45K. The major technological breakthrough in terms of cosmetics, noise performance and operating temperature was achieved by switching the growth technology from LPE (Liquid Phase Epitaxy) to MOVPE (Metal Organic Vapor Phase Epitaxy) using optimized heterostructure designs with a wide bandgap absorber region and a narrow bandgap gain region. This development is still ongoing, targeted to higher quantum efficiency, high APD gain, fast response, low dark current and panchromatic response. LPE arrays and a complementary NIR e-APD development carried out at SOFRADIR which is based on molecular beam epitaxy (MBE) already offer panchromatic response [4].

2. SAPHIRA MULTIPLEXER AND ESO TEST RIG

Even though early results were obtained with λ_c=2.5μm NIR eAPD prototype arrays on the SWALLOW ROIC developed for laser gated imaging, the special requirements of adaptive optics and interferometry with multiple windows and low readout noise at high frame rates could only be met by developing the new SAPHIRA ROIC, which is described in more detail in a previous paper [10]**.** The SAPHIRA ROIC has a format of 320x256 pixels and 32 parallel video outputs operating at 5 MHz. The 32 outputs are organized in such a way that they read out 32 adjacent pixels in a row at the same time. The readout time of a full frame is 500μs allowing frame rates of 1 kHz for double correlated sampling. With this readout topology, windowed readout schemes benefit from the multiplex advantage of 32 parallel channels. This is one of the key features of the SAPHIRA ROIC which helps to achieve the lowest readout noise. Depending on the size of the window many frames can be read out nondestructively with typical integration times of 1 ms, to reduce the readout noise even further with Fowler sampling. A 10 MHz 32-channel ADC board in the NGC detector front end electronics allows real–time digital filtering and Fowler preprocessing in the FPGA of the ADC board to limit the required bandwidth of the fiber link to the real time computer.

The test setup used to evaluate the eAPD arrays was also described in an earlier SPIE paper [10]. A test camera cooled by a closed cycle cooler allows operation of the detector at temperatures of 40K. The telescope focus is in front of the entrance window outside the camera at room temperature. Therefore, a test pattern such as a grid of holes illuminated by an extended blackbody can be used to generate a pattern of calibrated flux on the detector. The test pattern is imaged by the cryogenically cooled f/11 Offner relay onto the detector. Two cold filter wheels inside the camera are equipped with band-pass and neutral density filters.

3. LIQUID PHASE EPITAXY APD ARRAYS

The first near infrared (NIR) eAPD arrays grown by Liquid Phase Epitaxy on a prototype multiplexer (SWALLOW) have demonstrated the feasibility of electron avalanche multiplication to break the CMOS noise barrier. The dark current scales with the width of the bandgap. Reducing the cutoff wavelength from λ_c = 4.5 μm to 2.5 μm brought the dark current down to levels which are negligible at frame rates of 1 kHz. To collect avalanched electrons n-on-p structures are required. The LPE arrays are annular structures which operate with lateral collection of charge generated by photons in the p-type absorber region. The charge collected by diffusion is then amplified in an annular gain region around the n side of a metalized hole making the contact to the multiplexer [5][6]. The hole in the center of the pixel is metalized to make the contact to the ROIC. The so-called LPE loophole structure is shown on the left side of Figure 2, this is compared to the MOVEPE/mesa structure, also shown and described in chapter 4.

Early results with LPE arrays on a prototype multiplexer were encouraging [9]. However, the first LPE arrays hybridized on the SAPHIRA ROIC did not meet the expectations raised by the prototype results. The number of noisy pixels and the nonuniformity increased rapidly above 6V bias even when cooling the array down to temperatures of 40K. The bottom left side of Figure 1 shows a noise map at an operating temperature of 40K with an APD gain of 25.

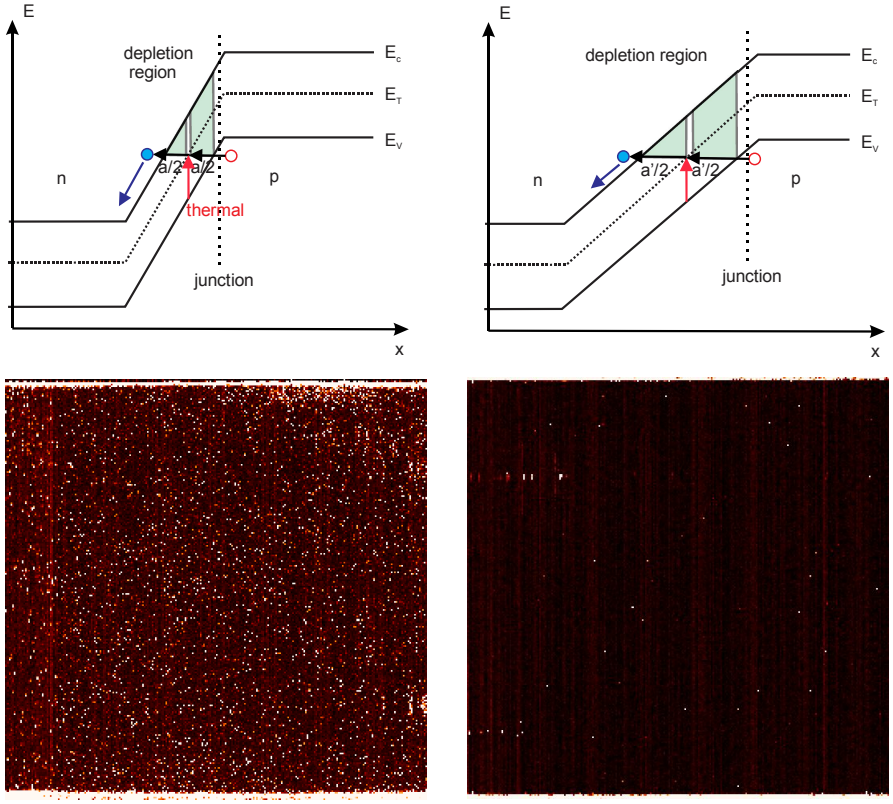

Figure 1 Top: Band diagrams of LPE eAPD arrays. Bottom: Noise maps with cut levels 0 to 20 erms at an integration time of 575 µs, APD gain of 25 and operating temperature of T=40K. Top left: Narrow depletion width with large electric fields and narrow potential barrier risking trap assisted tunneling defects. Bottom left: Corresponding noise map. Top right: Wide depletion width with reduced electric fields and wide potential barrier for reduced trap assisted tunneling. Bottom right: Corresponding noise map.

The cut levels of the noise maps at the bottom of Figure 1 are 0 to 20 electrons rms. The large number of noisy pixels probably reflects a high dislocation density. Analysis showed that the bad pixels are mainly caused by trap-assisted tunneling (TAT) and originated around the junction region. Since the tunneling probability decreases exponentially with the height and the width of the potential barrier, an increase in the width of the depletion region where the APD gain occurs reduces the probability of trap-assisted tunneling. This is schematically shown by the top two energy band diagrams of Figure 1. The corresponding noise maps at the bottom of Figure 1 show the dramatic reduction of noisy pixels for the larger depletion width at high APD gain. LPE arrays with large diodes on the SAPHIRA multiplexer present a technological breakthrough and achieve the expected results of 2.5 electrons readout noise for the full frame with double correlated sampling and 0.8 electrons rms with Fowler-8 for a 96x72 pixel subwindow. However, the arrays have to be cooled to operating temperatures of 40K to achieve this performance.

4. METAL ORGANIC VAPOR PHASE E-APD HETEROJUNCTION ARRAYS

The LPE loophole structure is the most mature technology for APD arrays. The technology has some merits such as low doping levels, panchromatic spectral response and a beneficial geometry for avalanching. However, diodes become leaky at high bias voltages and require deep cooling down to 40K. In the past ten years Selex have replaced LPE technology with Metal Organic Vapour Phase Epitaxy (MOVPE) grown on GaAs substrates [7][8].

The first MOVPE array delivered to ESO was a homojunction with uniform cutoff wavelength. With this device all the required processes were put in place which are needed to manufacture MOVPE such as the photolithographic masks and indium bump bonded SAPHIRA wafers. However, breakdown voltages, defect levels, and the dark current of MOVPE homojunctions were not as good as the best LPE arrays.

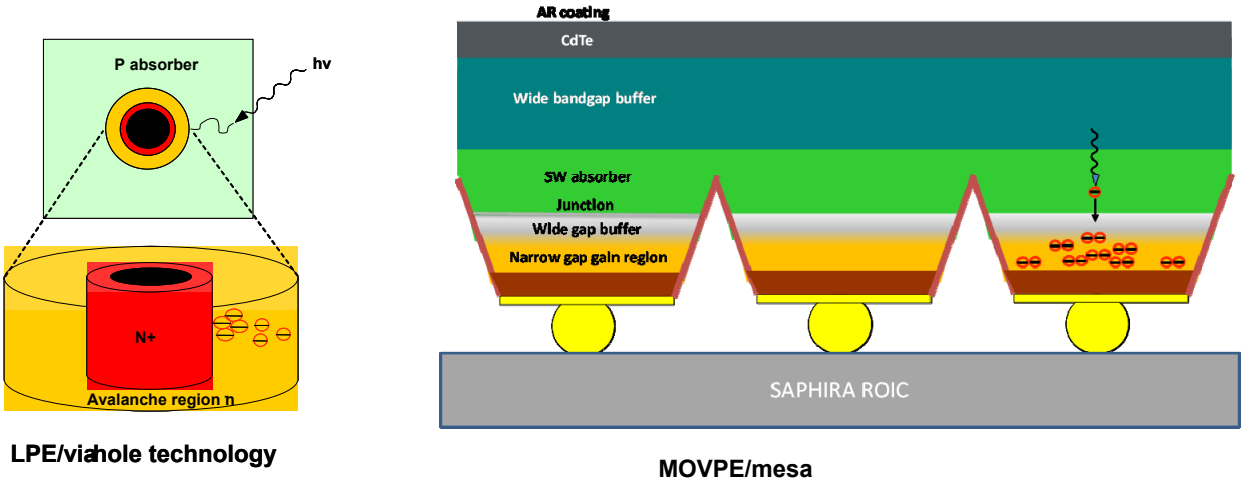

Figure 2 Left: Diode structure of liquid phase epitaxy (LPE) array. Right: Diode structure of metal organic vapour phase epitaxy (MOVPE)

During 2013 ESO were joined by NRC Herzberg Institute of Canada to fund Selex ES to manufacture custom designed heterojunctions. In 2014 a consortium of ESO, University of Hawaii and the UK ATC have funded Selex to develop special aspects of the MOVPE growth process to enhance the device performance for astronomy. The process of defining the parameters to be improved is still underway as better data emerges. There is a performance envelope embracing avalanche gain, QE, response time, cosmetics and noise figure as a function of the APD design, processing technology, operating temperature and bias voltage. The strategy during Q1 and Q2 2014 has been to run MOVPE batches with experimental features to progress our understanding. The latest designs are currently being evaluated and there is very much work-in-progress. However, it will be shown below that some features stand out.

Metal Organic Vapour Phase Epitaxy (MOVPE) of HgCdTe was developed for the thermal imaging market at Selex ES. MOVPE alternates the growth of CdTe and HgCd and the bandgap of HgCdTe after interdiffusion is determined by the ratio. Low cost GaAs substrates provide a wafer-scale process suitable for large area arrays. Dopants are introduced on the CdTe cycle so the doping levels are independent of the bandgap. Iodine is used as a donor and arsenic as an acceptor. Initially it was believed that MOVPE would be unsuitable for APDs because of potentially high levels of misfit dislocations that are usually associated with junction breakdown currents. However work funded by ESO showed that bandgap engineering, a high optical absorption coefficient and a properly optimized device design more than compensate for the presence of weak misfit dislocations [1]. The work in 2013 resulted in several wafers of MOVPE material and the best science-grade arrays were delivered to ESO and the NRC Herzberg Institute (HI) of Canada. This represented the state of the art for the basic MOVPE process as developed for thermal imaging. Since that time ESO, HI and the University of Hawaii have been evaluating these arrays to define the limitations and prepare for specific research on the MOVPE process to advance the performance for astronomy [12][13][14]. Since MOVPE allows the band structure and doping to be controlled on a 0.1µm scale it provides more flexibility for the design of diode structures. The bandgap can be varied for different layers of $Hg_{(1-x)}Cd_xTe$ by varying the stoichiometry x of the alloy during the growth process to build heterojunctions.

4.1 Energy band diagram of MOVPE heterostructure

The band diagram of the device structure is illustrated in Figure 3 and a schematic of the device design is shown on the right side of Figure 2. Placing the junction in a wide band-gap buffer gives: low trap- assisted tunneling current, low trap-related thermal current and immunity from weak misfit dislocation loops. The exact design of this buffer is critical

and confidential. The absorber and the gain region are decoupled so each can be optimized separately. The gain region is made narrow bandgap to give high gain per volt but a compromise is needed here to avoid too much stray light or dark current. One of the benefits of the heterojunction design is that dark current is generated in the gain region and only experiences a fraction of the voltage drop. The difference between 12V and 6V is a factor of x25 so there is a differential in the gain experienced by photons and that experienced by dark current. Future designs could emphasize the differential for photon counting applications. Each pixel is electrically isolated by a mesa slot that extends though the absorber to eliminate lateral collection. The optical crosstalk, MTF and pixel inter-capacitance of MOVPE arrays are exceptional. The sidewalls are coated with a CdTe layer that is inter-diffused at high temperature. The widening of the bandgap around the edges of the absorber effectively separates carriers from surface states and minimizes junction currents where the junction intercepts the sidewall. The high temperature anneal also promotes long term stability at high operational temperatures. HgCdTe is the only infrared material that permits so-called hetero-passivation and it has a strong impact on the reverse-bias breakdown in APDs.

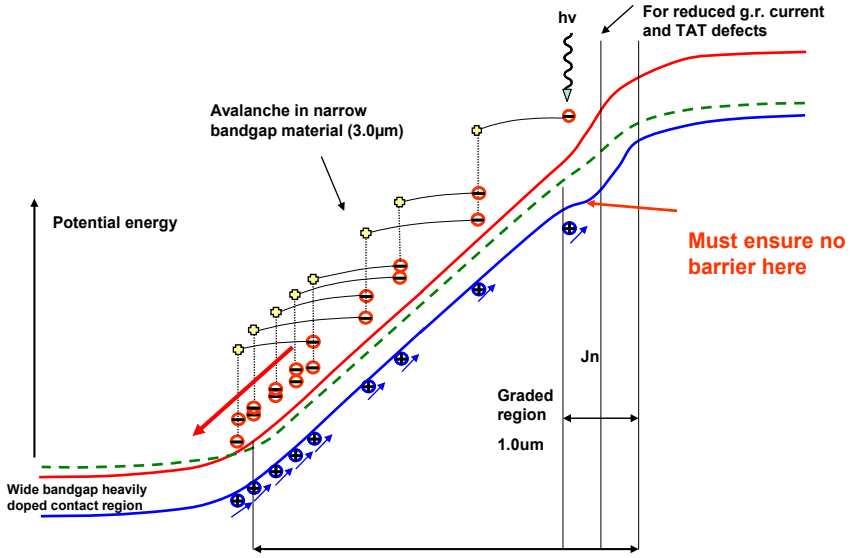

Figure 3: Band diagram of MOVPE heterostructure eAPD array. Wide bandgap in absorber region and the junction on the right side. Narrow bandgap in gain region for maximum APD gain at small bias voltages.

So far two MOVPE arrays have been evaluated at ESO. The first array called Mark 3 had an arsenic doping concentration of 3e16 cm^{-3}. The doping concentration of the second array called Mark 5 was an order of magnitude lower.

4.2 Cosmetic quality

To our surprise, even at a temperature of 85K the cosmetic quality of Mark 3, the first MOVPE heterostructure delivered to ESO, is stunning. The widening of the bandgap at the junction and the separate optimization of the absorber and the gain region very effectively suppressed the number of defects caused by trap-assisted tunneling. This is shown in Figure 4, where the flat-fields of the best LPE array and the first MOVPE heterojunction are compared. At the maximum bias voltage of 12.1 V, when the APD gain in H-band is 76, on the heterostructure shown in the right image of Figure 4 there are only 20 pixels, which have a signal 30% larger or smaller than the mean signal. Operating arrays at T=85K reduces system complexity. If no deep cooling is needed the detector can be operated without pulse tube cryo coolers. This is a big advantage for interferometric applications which are sensitive to vibrations.

4.3 Nodal capacitance

The transfer gain of the SAPHIRA ROIC, defined as the ratio of the voltage change at the video output and the integrating node of the unit cell, was measured to be 0.62. The capacitance of the integrating node at a moderate bias voltage of 2.61 V was derived from the variance versus signal method. With a gain of 11.22 electrons/ADU derived from the photon transfer curve and 3.81 μV/ADU, back referred to the integrating node in the unit cell of the pixel, then the

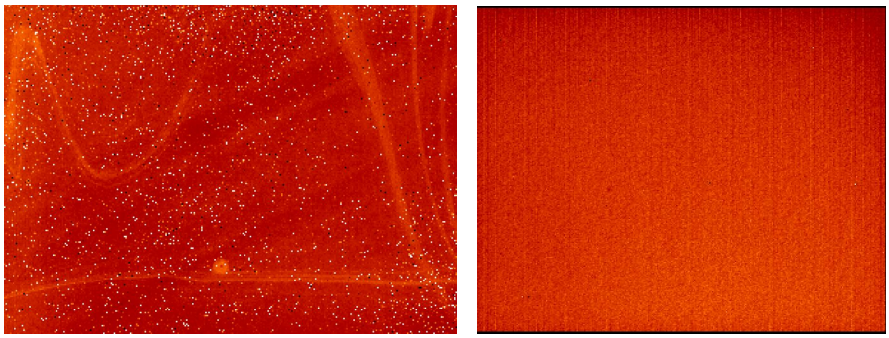

Figure 4: Flatfields in K-band. Left: LPE eAPD array at APD gain of 16.6 and operating temperature of T=45K. Right: MOVPE heterostructure at APD gain of 59 and operating temperature of T=85.

total capacitance is derived to be 29.4 fF. This is equivalent to a voltage change of 5.44 μV per electron without APD gain at a bias voltage of 2.61V. The capacitance increases to 49.4 fF at a bias voltage of 0.62V.

4.4 Quantum efficiency

QE is difficult to measure accurately but Figure 5 shows measurements based on conversion gains determined by the photon transfer method. The quantum efficiency was measured in H and K band at a bias voltage of 620 mV without APD gain. The integration time was kept fixed and the flux was changed by changing the blackbody temperature. The quantum efficiency was derived from the slope of the regressional fit to data points showing the number of electrons versus the number of photons arriving at the detector. A noticeable feature is the drop of QE with temperature. The Mark 3 device has an absorber doped to 3e16 cm^{-3} with arsenic. The QE drop with decreasing temperature implies the activation of an electron recombination trap. A potential candidate is un-ionized arsenic since the proportion of un-ionized arsenic rises as it freezes out at lower temperatures and wider bandgap.

To explore the possibility of an arsenic-related trap Selex developed a low arsenic doping growth technique which involved an experimental layer with many combinations of dilution techniques. This was analyzed using SIMS and Hall measurements at Southampton and QMSA analysis at the University of Western Australia. A method was developed to control doping to low-10^{15} cm^{-3} levels. An APD layer was grown with arsenic doping an order less than the Mark 3 array having an arsenic concentration of 3e10^{15} cm^{-3}. The layer is known as Mark 5.

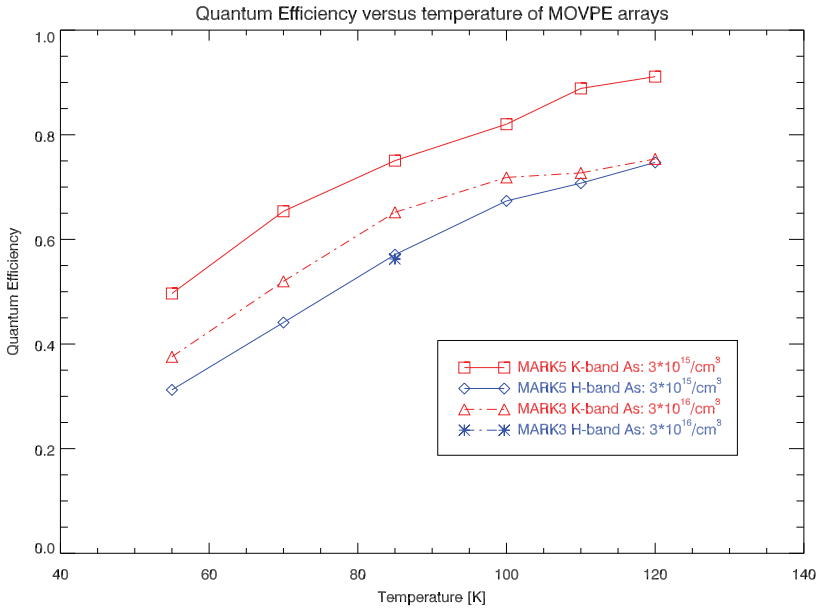

Figure 5 Temperature dependence of quantum efficiency of SAPHIRA MOVPE eAPD heterostructure arrays. Red squares MARK 5 K-band. Blue diamonds: MARK 5 H-band. Red triangles: MARK 3 K-band. Blue asterisk: MARK 3 H-band.

Figure 5 shows that the trend of QE with temperature is unaffected by the arsenic doping. Some of the other aspects of Figure 5 can be understood from absorption depth. H band photons are absorbed closer to the surface and the resultant electrons have a longer distance to diffuse to the junction. This is a qualitative explanation for K band having higher QE. The most important conclusion from the Mark 5 work is that the arsenic doping is not directly responsible for the QE drop at low temperature. In H-band the QE of Mark 3 and Mark 5 are almost the same and the arsenic doping has no effect on the QE.

4.5 Dark current

The dark current of Mark 3 at a bias voltage of 10V back-referred to the unit cell sensing node is shown in Figure 6. It depends on the multiplexer supply voltage VDD, which indicates a glow problem for low flux applications. By reducing VDD from 6.4 V to 5 V the dark current drops from 95 e/s/pixel to 44 e/s/pixel. This value is adequate for wavefront sensing with integration times of a few ms but it is too high for low flux scientific applications requiring dark currents of a few 10^{-2} e/s/pixel.

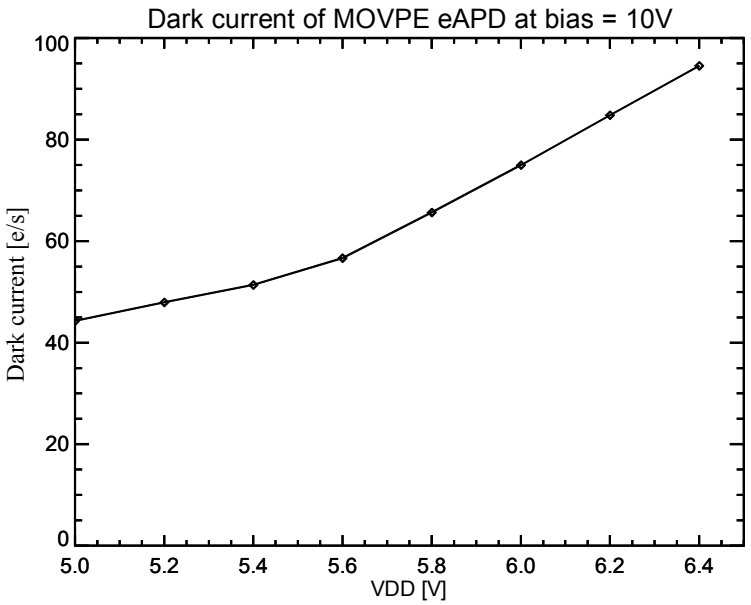

Figure 6 Dark current at bias of 10V for different supply voltages VVD.

4.6 APD gain

The APD gain shown in Figure 7 was normalized to one at a bias voltage of 620 mV. For Mark3 the APD gain is higher in H band than in K band due to the partial APD gain of long wavelength photons, as explained below when describing the noise figure. It is difficult to disentangle the effect of the voltage dependence of the nodal capacitance from the avalanche effect and their contributions to the overall gain at moderate bias voltages. In this voltage regime the overall gain consists of two components. One component is the reduction of the diode capacitance with increasing bias. This reduction of the nodal capacitance also increases the signal response. The second component is the onset of APD gain. At higher bias voltages when the diode is fully depleted the gain is entirely due to the avalanche effect.

The APD gain of Mark 3 is higher than the gain of the LPE array. Mark 5 had a much lower avalanche gain than Mark 3 despite similar gain region dimensions and doping levels. The main difference was the very lightly doped P-region. Poisson analysis showed that the likely explanation was that the avalanche gain process only became effective in the gain region. So the voltage dropped across the depletion region in the P-region was wasted. A qualitative explanation is that electron scattering or trapping is higher in this region so electrons are not able to start the process of gathering energy.

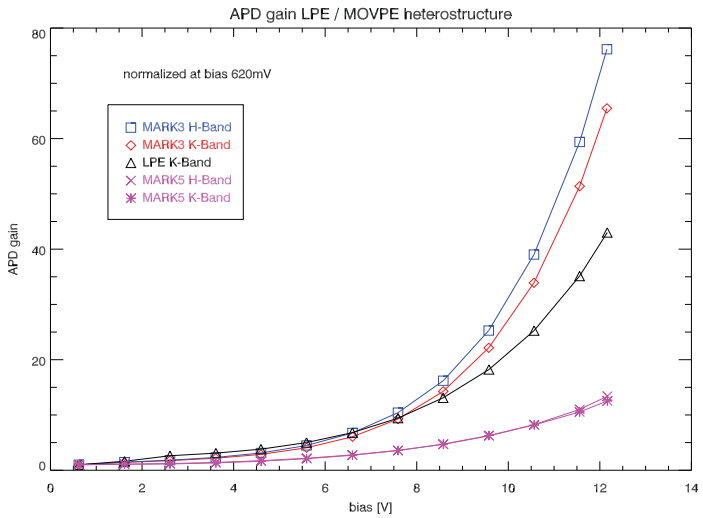

Figure 7: APD gain versus bias voltage for the MOVPE arrays Mark 3 and Mark 5 and an LPE array for comparison. Mark 3: H-band (squares) and K band (diamonds); APD gain of LPE array in K band (triangles); Mark 5: K-band (asterisks *) and H-band (crosses X).

4.7 Speed of response

The first measurements with the MOVPE array based on the Mark 3 design were carried out at an operating temperature of 53 K. At this temperature the speed of response of a chopped signal is quite slow. As can be seen in Figure 8, which shows a chopped signal, the speed of the detector response increases with increasing temperatures. At a temperature of T=55 K the rise time of the detector signal is 34 ms. If the detector is operated at a temperature of T=85 K the rise time is less than 2.34 ms, which was the time interval between two full frame readouts.

Speed of response can be important in fast frame rate applications, for instance wavefront sensors need to operate at thousands of frames per second. Also there are applications that require both high speed and low dark current, such as photo counting, where the detector is likely to be cooled to low temperatures. The Mark 3 detector showed a strong dependence of response time on temperature. For the astronomy community this is a clear development topic for the APD technology. The chopped signal of the low doped array based on the Mark 5 design is shown in Figure 9. It demonstrates impressively the faster response time at an operating temperature of T=55 K. The rise time of the signal is less than 181 µs which is the time interval between two readouts of the 48 spectra taken with Fowler sampling in the fringe tracking mode, reading out 32 x 24 pixels using the window mode of the SAPHIRA array. The integration time was 90.5 µs.

The process of deconvolving the QE and response time effects in Mark 3 and 5 is work-in-progress. Reducing the arsenic doping in the absorber of Mark 5 had a strong effect on the response time but not the QE, yet the activation energies of

the two effects were similar.

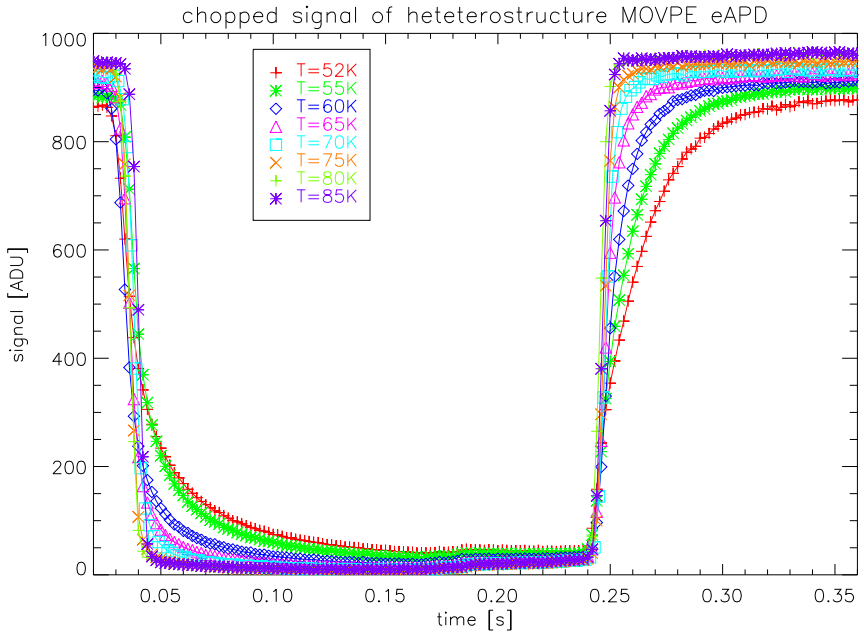

Figure 8 Chopped signal taken with Mark 3 heterostructure at temperatures between 53 and 85 K. Rise time at T=55 K is 34 ms. Rise time at T=85 K is < 2.34 ms which is the time interval between two full frame DCS readouts (one DCS with 2 frames)

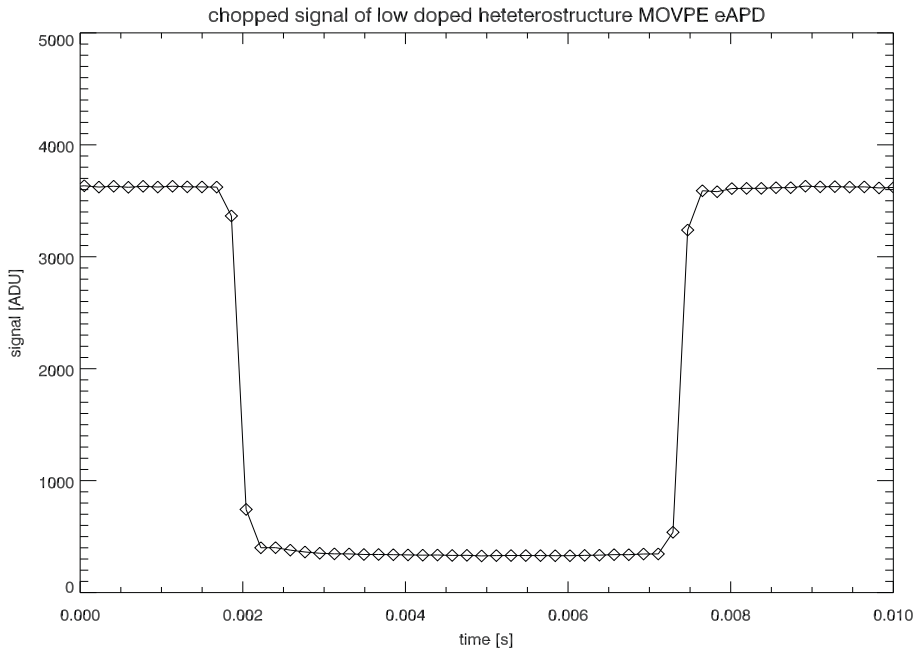

Figure 9 Chopped signal at an operating temperature of 55K taken with MARK 5 (low doped arsenic)

4.8 Excess noise

The noise figure of APDs describes the noise associated with the gain process. If the noise figure is larger than unity the noise increases faster than the signal at high APD gain. Hence the ultimate signal to noise benefit of avalanche gain is degraded. The noise figure can be determined by plotting the inverse conversion gain obtained from the variance versus signal method as a function of reverse bias voltage and division by the APD signal gain. In Figure 10 the MOVPE noise figure is plotted versus APD gain for H and K-band of MARK 3 and compared with the noise figure of LPE arrays. Sometimes the excess noise factor is defined as the square root of the noise figure, but the noise figure in Figure 10 was plotted without taking the square root. In all silicon devices with electron multiplication the noise figure is larger than 2.

Because of the low noise figure, HgCdTe with panchromatic response has the potential to outperform silicon detectors. The noise figure of the MOVPE array is 1.23 up to an APD gain of 79 in H-band but in K-band it rises to 1.37 at an APD gain of 59. This indicates that long wavelength photons penetrate deeper into the diode and are also absorbed in the gain region. Hence the photon generated charge experiences only partial APD gain. Since the absorption is a random process, photons being absorbed at different depths in the gain region experience different APD gains. This contributes to APD gain noise and increases the noise figure. The shorter wavelength photons are absorbed higher in the structure in arsenic doped p-side of the diode junction and must travel the furthest to reach the gain region. They experience the full APD gain which is noiseless. To achieve the optimum performance the noise figure has to be reduced for K-band photons by increasing the thickness of the absorber layer, thus ensuring that these photons experience the full APD gain. This will improve the noise figure in the K-band to values comparable to those of the H-band.

The low doped array Mark 5 shows a high excess noise factor. This may be the result of trapping and scattering of photo-electrons before they enter the gain region and the spread of energies results in a very high noise figure.

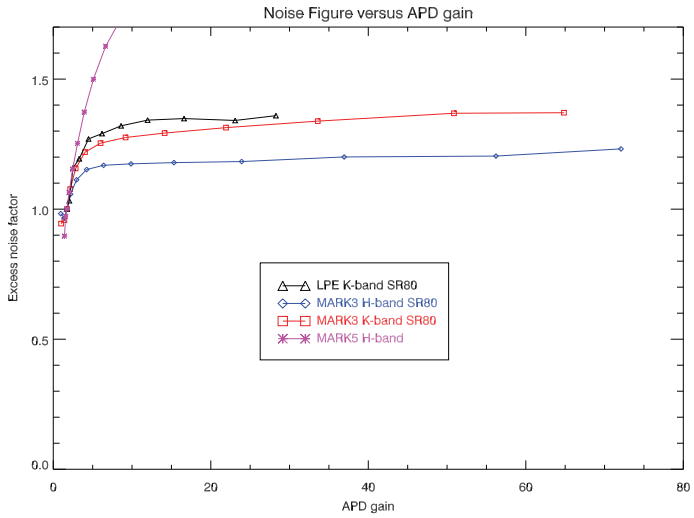

Figure 10: Noise figure of eAPDs versus APD gain. Red squares: MOVPE heterostructure in K-band. Blue diamonds: MOVPE heterostructure in H-band. Black triangles: LPE in K-band.

4.9 Readout noise and sensitivity

Since Mark 3 is the most sensitive array, all results on noise and sensitivity have been obtained with this array. In Figure 11 the noise histogram of a dark exposure taken with a simple double correlated sample is shown. The array was operating at the maximum APD gain which is 59 in K-band and 79 in H-band. The noise histogram peaks at 0.8 electrons rms for K-band photons. The integration time was 1.17 ms. The corresponding noise value for H-band photons is 0.6 electrons rms because of the higher APD gain in H. Figure 12 shows our test pattern, a grid of holes inserted into the telescope focus which is reimaged onto the detector by the f/11 Offner relay. The test pattern is uniformly illuminated with an extended blackbody at a temperature of 70ºC and observed with the H band filter. The flux in the holes of the test pattern is 1.12 photons/ms per pixel or 0.52 electrons/ms per pixel. The integration time is 1.17ms. The left image of

Figure 12 shows a single exposure, and the right image is the average of 12 chop cycles at a chopping frequency of 10 Hz. The left image clearly demonstrates that the sensitivity is sufficient to detect single photons in a single DCS frame at the maximum APD gain.

The main advantage of the SAPHIRA readout topology only becomes apparent when reading out small subwindows as are often needed for low order AO systems and fringe trackers. For example, the GRAVITY wavefront sensor has 9x9 sub-apertures with 8x8 pixels per sub-aperture [11]. Therefore, a window of only 96x72 pixels needs to be read out.

Because of the ROIC topology, the number of pixels in the fast readout direction has to be a multiple of 32. In Figure 13 the readout noise is plotted versus the number of nondestructive samples for different APD gains ranging from 25 to 79. The integration time for the data points of Figure 13 having less than 8 nondestructive readouts (4 Fowler pairs) is fixed to 500µs to limit the number of interrupts for the host computer. For 16 (Fowler-8) and more readouts the integration time increases with the number of nondestructive readouts. The integration time is 1.17 ms for 32 readouts (16 Fowler pairs) and 37.5 ms for 1024 readouts. For integration times longer than 19 ms or more than 256 Fowler pairs the readout noise becomes independent of the APD gain. The readout noise is dominated by the instrumental photon background in our camera. Since the gain region has a narrow bandgap the detector is still sensitive to thermal radiation up to λ>3.5 µm, however with low efficiency. The noise data were taken at a detector temperature of 85 K. This measurement will have to be repeated at lower detector operating temperatures and with the detector covered by a cold plate to shield it from the instrumental thermal background. With Fowler-16, an APD gain of 79 and an integration time of 1.17 ms, the readout noise is 0.2 electrons rms. With this performance the read noise of the GRAVITY wavefront sensor is negligible and single photons can safely be detected.

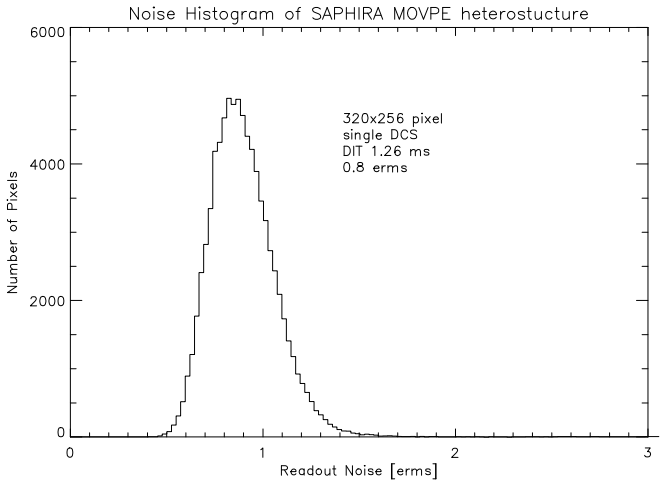

Figure 11: Noise histogram of heterostructure eAPD for full fame (320x256 pixel) readout and single DCS. Readout noise 0.8 electrons rms. Integration time 1.26 ms.

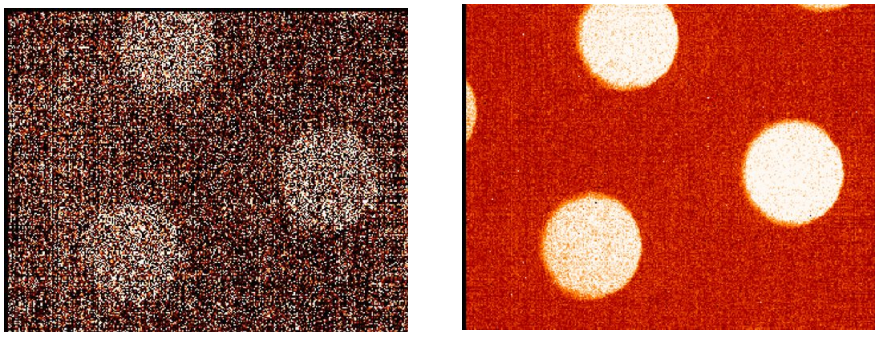

Figure 12: H-band test pattern with signal difference of 1.3 photons or 0.59 electrons in integration time of 1.17ms. Left: Single exposure. Right: Mean of chopped image.

4.10 Shot noise limited operation of GRAVITY WFS for on-sky flux conditions

For the GRAVITY instrument the Coude focus of each of the four VLT telescopes has to be equipped with the Coude Infrared Adaptive Optics system called CIAO. In each telescope the CIAO system corrects the wavefront which is distorted by the atmospheric turbulence. CIAO is based on a Shack-Hartmann wavefront sensor operating in the wavelength range from 1.4 µm to 2.4 µm with 9x9 sub-apertures each having 8x8 pixels. The f-number of the lenslet array is f/10.91. This is almost identical to the f-number of the Offner relay in our test camera IRATEC which is f/11.

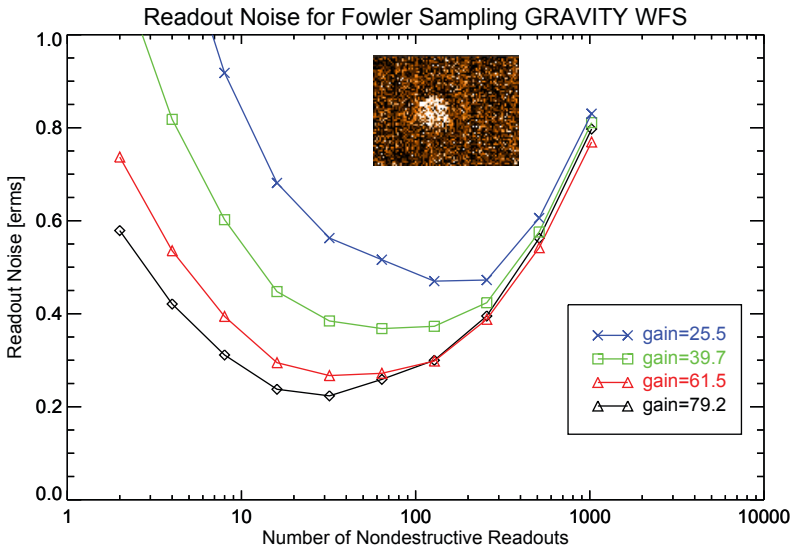

Figure 13 Readout noise of the 96x72 pixel sub-window of the GRAVITY wavefront sensor with Fowler sampling as a function of the number of nondestructive readouts at different APD gains. Integration time increases with the number of nondestructive readouts. The inserted image in the top right corner shows a single 1ms exposure imaging a circular test pattern having a signal of 1 electron/ms/pixel.

The average temperature in the telescope is 15ºC. Figure 14 shows the number of photons per millisecond per pixel per µm emitted by an extended blackbody at a temperature of 15ºC, when observed through the bandpass filter of the GRAVITY CIAO system (red curve) or looking through the K-band filter of the IRATEC test camera (blue curve). In IRATEC the calculated flux is 2.91 photons/ms/pixel. In the GRAVITY CIAO system the flux is 9.91 photons/ms/pixel. Therefore, the flux measured with our IRATEC test camera corresponds to the flux expected with the CIAO system on-sky if the overall emissivity ε of sky, telescope and the optical train is ε=0.29.

In order to verify shot noise limited operation in the lab for conditions to be encountered on sky with the CIAO system of GRAVITY a cold mask with a hole having a diameter of 2 mm was mounted directly in front of the detector. The mask is shown in Figure 15. Looking through the cold hole at a blackbody at a temperature of 15ºC the detector sees the same flux as encountered on sky with the lenslet of CIAO. For detector pixels located outside the hole the flux is sufficiently low that the photon shot noise is negligible in comparison to the detector readout noise.

The hole in the cold mask can be seen in the noise map as a circular area of the increased noise if the photon shot noise becomes dominant, whereas the noise outside the hole is pure readout noise. The circular area of increased noise proves that the detector is operating in the photon shot noise limited regime irrespective of any calibration issues.

Figure 16 shows the signal and noise maps obtained with the IRATEC test camera and the mask with the hole mounted in front of the detector. The detector integration time was 1ms and the blackbody temperature 15ºC. The two images on the left represent the signal and the two images on the right are the corresponding noise maps. The large images have been taken with double correlated sampling reading out the full frame. The small images were obtained with Fowler sampling using the windowed readout with 96x72 pixels as needed for the CIAO system in GRAVITY. The Fowler sampling with 6 Fowler pairs was combined with subpixel sampling averaging 3 ADC conversions per pixel readout.

The Fowler processing is performed in the FPGA of the ADC board in our NGC controller. The APD gain in Figure 16 is increasing from the top row with an APD gain of 1.82 to bottom row with an APD gain of 76.2. The noise maps on the right half of Figure 16 clearly demonstrate that the total noise becomes photon shot noise limited at an APD gain >20 for DCS and at an APD gain > 10 for Fowler sampling. At the maximum APD gain of 76.2 both readout modes are fully shot noise limited assuming conditions representative for on-sky operation in CIAO. The measured noise under the hole is 1.36 erms. Assuming a quantum efficiency of 65 %, the photon shot noise is 1.37 erms. The measured readout noise outside the hole is 0.92 erms for DCS and 0.57 erms for Fowler sampling using the window mode. With this readout noise the photon shot noise limited operation is possible for integration time as short as 112 µs.

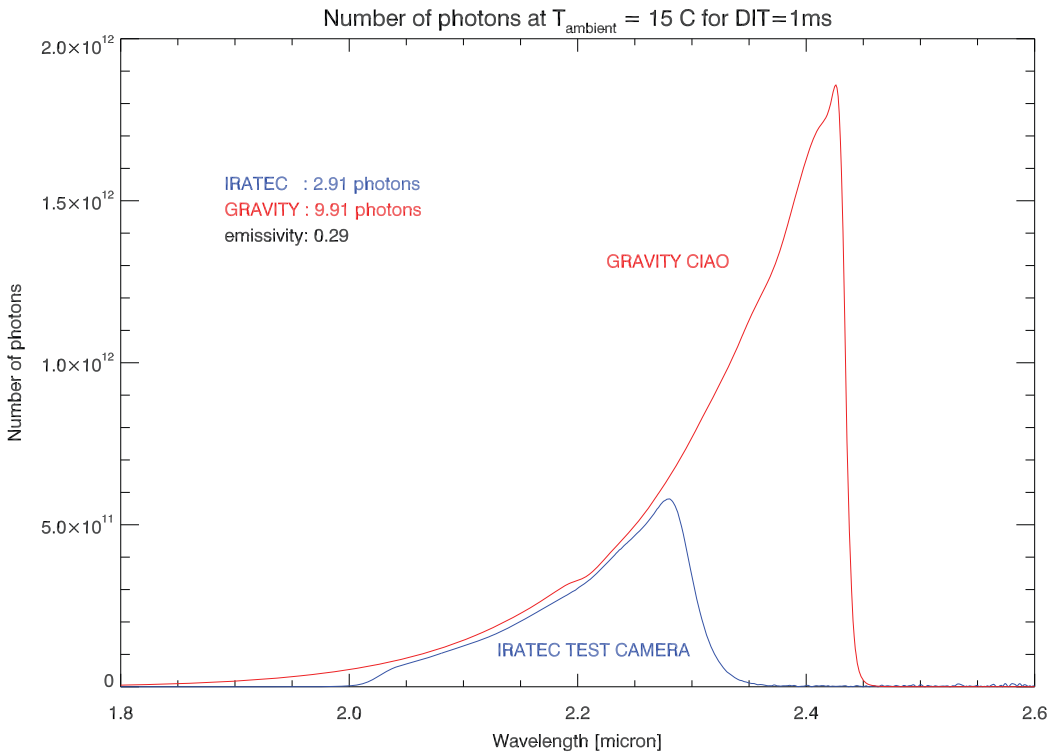

Figure 14 Number of photons per millisecond per pixel per µm emitted by an extended blackbody at a temperature of 15ºC and observed through the bandpass filter of the GRAVITY CIAO system (red curve) or through the K-band filter of the IRATEC test camera (blue curve). The f-number of both systems is f/11. IRATEC: 2.91 photons/ms/pixel. GRAVITY CIAO: 9.91 photons/ms/pixel. The flux in IRATEC corresponds to expected flux on-sky in the CIAO system of GRAVITY assuming an overall emissivity ε of sky, telescope and optical train of ε=0.29.

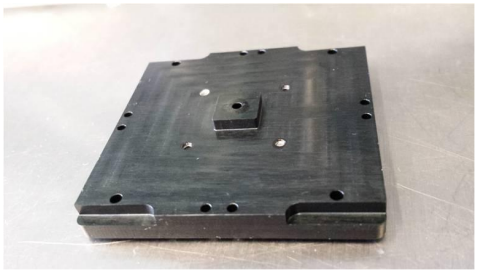

Figure 15 Cold mask in front of detector to measure photon shot noise and readout noise

Further improvement of the sensitivity can only be achieved by reducing the emissivity of the telescope and the optical train to the Coude focus, which may be larger than the value of ε=0.29 assumed here. An alternative would be to limit the bandwidth of the bandpass filter used in CIAO on the long wavelength side to reduce the thermal background optimizing the signal to noise for the low readout noise of the SAPHIRA detector.

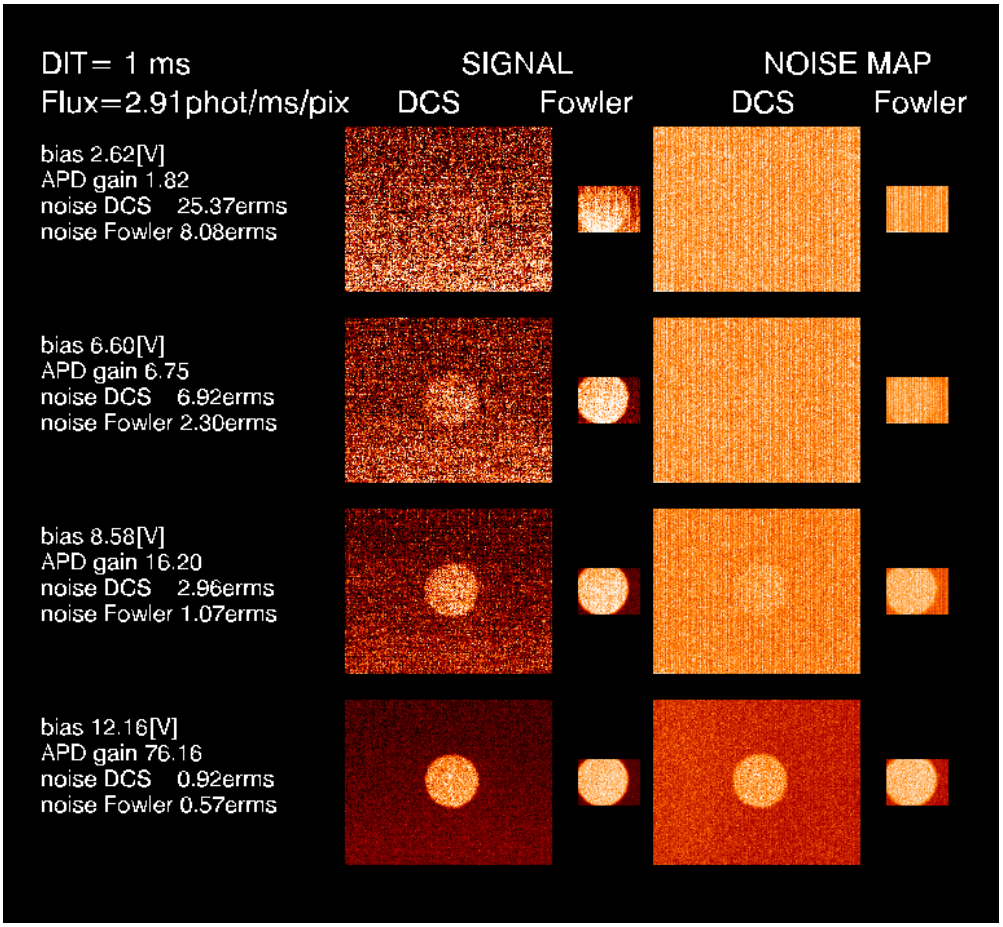

Figure 16 On-sky sensitivity of SAPHIRA array expected for an integration time of 1ms with double correlated sampling of full frame and with Fowler sampling of 96x72 pixel window. Two images on the left: signal maps. Two images on the right: noise maps. Top to bottom: increasing bias and APD gain with readout noise measured without illumination. Photon shot noise limited operation with DCS at APD gain >20 and with Fowler at APD gain > 10. Fully photon shot noise limited operation at maximum APD gain for both DCS and Fowler sampling.

5. OUTLOOK

A revision of the SAPHIRA ROIC is planned to implement the read-reset-read mode per row. In this mode the array is integrating photons also during readout. This will increase the stare efficiency at the highest frame rate to almost 100%. Some fine-tuning of the unit cell and enhanced output voltage referencing will also be included in the revised design.

In the standard MOVPE process developed for thermal imaging a thick buffer layer comprising a sequence of HgTe and CdTe cycles is used to turn over misfit dislocations arising from the crystal lattice mismatch of GaAs. The equivalent cut-off wavelength of the buffer layer is 1.35 µm. It reduces the QE in J band (1.15-1.35 µm) and limits the useful spectral range of the MOVPE eAPD arrays tested so far to wavelengths between 1.35 µm and 2.5µm. Investigations are ongoing at Selex ES to find an alternative buffer layer with transparency in J band. The buffer layer has the role of improving the crystallography and so the growth morphology is of key interest. Wide bandgap MOVPE is prone to lose morphology and the use of a real-time laser interferometry growth monitoring tool during dedicated test runs provided instantaneous feedback. Growth rate determination for the HgTe and CdTe components is a key driver to target the composition when the growth conditions are changed. The growth can be monitored in real time by observing the laser interferometer's ¼ wavelength turning points. This allows multiple parameter changes per run to be evaluated as long as

morphology is not degraded by the choice of parameters. For any change in MOVPE conditions then the correct growth rates can be determined rapidly. By this technique a new buffer layer was developed with J band transparency.

To prove the buffer layer is suitable for APD devices it is necessary to make devices and compare them with devices from conventional buffers. Selex has grown an experimental APD with J, H and K band sensitivity to compare with a control layer with normal H and K sensitivity. Devices will be evaluated in the third quarter this year. A broader spectral bandpass with more photons will improve the sensitivity of AO sensors.

If the detector dark current can be suppressed to levels below the photon generated current of Zodiacal light between the OH lines in high resolution spectrographs ($<10^{-2}$ photons/pixel/s), eAPD arrays become competitive with NIR science detectors such as the Hawaii-xRG family.

6. CONCLUSIONS

Increasing the depletion width of LPE eAPD arrays reduces defects caused by trap-assisted tunneling. Good cosmetic quality can be achieved by cooling them to temperatures of 40K. LPE arrays provide panchromatic response. The readout noise for a full frame using single double correlated sampling is 2.55 electrons rms.

A major breakthrough has been achieved by changing the growth technology to MOVPE eliminating the need for deep cooling. Devices can be operated at temperatures of 85K with 99.97% of operable pixels. The readout noise for the full frame using DCS is 0.8 electrons rms. For the GRAVITY WFS, the sub-window readout noise can be reduced to the negligible value of 0.2 electrons rms by Fowler-16 sampling at an integration time of 1.17ms. The sensitivity of the array is only limited by the Poisson statistics of the absorbed photons. For negligible readout noise the ultimate figure of merit, the noise equivalent number of photons is F/Q. The measured noise figure in the current device F is 1.2 at the maximum APD gain. Current MOVPE arrays have reduced QE at low temperatures.

Since the noise equivalent number of photons with APDs at high APD gain and negligible readout noise is F/Q the best figure of merit is achieved with the highest quantum efficiency and the lowest noise figure. Designing APDs is a compromise and reducing the arsenic doping has benefited the response time but at an unacceptable cost to the avalanche gain and noise figure. It had a remarkably small effect on QE implying that Selex ES need to revert back to the Mark 3 design (which was good in aspects such as gain and few defects) and find a new way to improve QE and response time. The behaviour of the response time and QE with temperature suggests a reduced electron mobility in flat field conditions and this is currently being investigated by QMSA analysis at University of Western Australia. A new generation of designs is currently being processed with bandgap and doping gradients in the absorber to provide better QE and response time at lower temperatures. This will be part of a wider program to develop APDs to serve a broader application range in astronomy and include for instance, devices with panchromatic response and dark current levels comparable to flux levels of ~ 10^{-2} photons/s/pixel as encountered in high resolution spectrographs. This may render noise free APDs for large science arrays.

For high speed low noise applications eAPDs already achieve subelectron readout noise and they have advanced to a technical readiness level adequate to deploy them in wavefront sensors and fringe trackers.

REFERENCES

[1] Finger G., Baker I., Alvarez D., Ives D., Mehrgan L., Meyer M., Stegmeier J., "NIR HgCdTe Avalanche Photodiode Arrays for Wavefront Sensing and Fringe Tracking", Scientific Detector Workshop 2013,Florence, Italy, edited Beletic J, Roth M., Amico P., to be published (2013)

[2] Rothman J, Mollard L, Gout S et al, "History-Dependent Impact Ionisation Theory Applied to HgCdTe e-APDs", Jn of Elec Mat, Vol 40, No 8, (2011).

[3] Kinch M.A, and Baker I.M, "HgCdTe Electron Avalanche Photodiodes", Chapter 21, Mercury Cadmium Telluride - Growth, Properties and Applications, published by Wiley, (2011).

[4] Feautrier, P. et al.,"Revolutionary visible and infrared sensor detectors for the most advanced astronomical AO systems", Proc SPIE, Vol 9148, to be published, (2014).
[5] Baker I.M, Crimes G.J, Parsons J.E. and O'Keefe E.S., "CdHgTe-CMOS hybrid focal plane arrays – a flexible solution for advanced infrared systems", *Proc. SPIE*, Vol 2269, p.636., (1994)
[6] Baker I.M. and Maxey C.D., "Summary of HgCdTe 2D array technology in the UK", *Jn. Elec. Mat*, Vol 30, No.6, p.682, (2003).
[7] Hipwood L.G, Jones C.L, Shaw C, et al, "Affordable high-performance LW IRFPAs made from HgCdTe grown by MOVPE", Proceedings of SPIE, **6206**, 10-1, (2006).
[8] Hipwood L.G, Jones C.L, Walker D, et al., *Proc. of SPIE,* Vol 6542, 65420I, (2007).
[9] Finger G., Baker I., Dorn R., Eschbaumer S., Ives D., Mehrgan L., Meyer,M., Stegmeier J., "Development of high-speed, low-noise NIR HgCdTe avalanche photodiode arrays for adaptive optics and interferometry", Proc. SPIE 7742, pp. 77421K (2010).
[10] Finger G., Baker I., Alvarez D., Ives D., Mehrgan L., Meyer M., Stegmeier J., Thorne P., Weller H, " Evaluation and optimization of NIR HgCdTe avalanche photodiode arrays for adaptive optics and interferometry ", Proc SPIE, Vol. 8453. 84530T, (2012).
[11] Eisenhauer F. et al., "GRAVITY: Observing the Universe in Motion", The Messenger, vol. 143, p. 16-24, (2011).
[12] Atkinson D., Hall D., "Characterization and applications of SAPHIRA HgCdTe APDs at the University of Hawai'I", Proc SPIE, Vol 9146, to be published, (2014).
[13] Buscher D, Finger G, Young J, Seneta E, "Optimisation of infrared eAPD detector readout for interferometry", Proc SPIE, Vol 9146, to be published, (2014).
[14] Hardy T., Burley G.,Baker I.,"Performance of SAPHIRA HgCdTe avalanche photodiode arrays", Proc SPIE, Vol 9146, to be published, (2014).